Clays Clay Miner., Vol. 70, No. 2:270–289, 2022
https://doi.org/10.1007/s42860-022-00185-6

ORIGINAL PAPER

Solubility of Calcined Kaolinite, Montmorillonite, and Illite in High Molar NaOH and Suitability as Precursors for Geopolymers

Nadja Werling · Jonas Kaltenbach · Peter G. Weidler · Rainer Schuhmann · Frank Dehn · Katja Emmerich

Accepted: 16 May 2022

Abstract Clays and clay minerals dissolve over a broad pH range, such as during sediment diagenesis and in a variety of applications, including nuclear waste storage, landfills, and geopolymer binders in the construction industry. The solubility depends on process parameters (pH, temperature, pressure, etc.) and material properties (phase content, clay mineral composition, particle size, etc.). Pretreatments such as calcination or severe grinding change the material properties and could enhance solubility, which is called activation. The aim of the current study was to determine the solubility of three different clay minerals after calcination (metakaolinite, metamontmorillonite, and metaillite) in high molar alkaline solutions (NaOH) up to 10.79 mol/L and pH = 14.73. Furthermore, the solubility of an $Al(OH)_3$ powder in alkaline solution (NaOH) was analyzed, as it can be used to adjust the Si:Al ratio of geopolymer precursors. The residues of the clay minerals after the alkaline treatment were investigated to disclose potential alterations in their phase contents. Based on the results of the thermal and alkaline activation, conclusions about the suitability as geopolymer precursors were made. All clay minerals showed an increase in solubility proportional to the concentration of the alkaline solution. The solubility decreased in the order metakaolinite > metamontmorillonite > metaillite. Thereby, dissolution was incomplete for all three clay minerals (<90%) after 7 days and congruent for metakaolinite and metaillite but incongruent for metamontmorillonite.

Keywords Alkaline activation · Calcination · Clay minerals · Geopolymer · Metaillite · Metakaolinite · Metamontmorillonite · Solubility

N. Werling (✉) · R. Schuhmann · K. Emmerich
Competence Center for Material Moisture (IMB-CMM), Karlsruhe Institute of Technology (KIT), Gotthard-Franz-Str. 3, 76131 Karlsruhe, Germany
e-mail: nadja.werling@kit.edu

J. Kaltenbach · P. G. Weidler
Institute of Functional Interfaces (IFG), Karlsruhe Institute of Technology (KIT), Hermann-von-Helmholtz-Platz 1, 76344 Eggenstein-Leopoldshafen, Germany

F. Dehn
Institute for Concrete Structures and Building Materials (IMB), Karlsruhe Institute of Technology (KIT), Gotthard-Franz-Str. 3, 76131 Karlsruhe, Germany

Introduction

Clay and clay mineral dissolution over a broad pH range takes place in natural systems, such as during sediment diagenesis and soil (trans)formation, in geotechnical applications including landfill liners (Kayabali, 1997; Rozalén et al., 2008) and geotechnical barriers of nuclear waste deposits (Charlet et al., 2017; Dohrmann et al., 2013; Güven, 1990; Madsen, 1998), in technical production processes or applications including during production of bleaching earths (Steudel et al., 2009a, b ; Valenzuela Díaz & Santos, 2001), and in construction materials (Khalifa et al., 2020; Shubbar et al., 2019). For construction materials, clays in their natural form or after thermal or mechanical activation are used as

rheology modifiers (Tregger et al., 2010), supplementary cementitious materials (Badogiannis et al., 2005), or precursors of geopolymers, and are subjected to solutions of various pH (Duxson et al., 2005; Werling et al., 2020).

Clay dissolution and formation of new phases is determined by material properties (phase content, clay mineral composition and structure, particle size, and microstructure) and process parameters (pH, activity of protons and hydroxyls, temperature, pressure, and saturation state of solution) (Amram & Ganor, 2005; Köhler et al., 2003; Nagy, 2018; Rozalen et al., 2009; Sato et al., 2005). Pretreatments such as severe grinding or calcination change the clay mineral structure, particle size, and microstructure and represent additional influence on dissolution characteristics. Typically, the temperature-dependent dissolution at a given pH follows the Arrhenius law. Dissolution rates decrease with increasing pH under acidic conditions, minimize at near neutral pH, and increase with increasing pH under basic conditions. This reflects proton-promoted dissolution at low pH, hydrolysis at intermediate pH, and hydroxyl-promoted dissolution at high pH (Rozalen et al., 2009). Proton exchange on interlayer positions of swellable clay minerals promotes the dissolution of smectites under acidic conditions (Janek et al., 1997; Steudel et al., 2009a, b). Alkaline dissolution is controlled mainly by dissolution of layer edges, whereas the basal surfaces are unreactive (Bauer & Berger, 1998; Kuwahara, 2006; Sato et al., 2003).

To elucidate the dissolution mechanisms and kinetics, research concerning the dissolution characteristics of clay minerals has been performed with a wide variation of different experimental setups in flow-through (Metz et al., 2005; Rozalén et al., 2008; Rozalen et al., 2009) or batch reactors (Bauer & Berger, 1998; Bauer et al., 1998; Carroll-Webb & Walther, 1988; Köhler et al., 2003; Zysset & Schindler, 1996). In batch reactors the solid/liquid ratios are fixed from the beginning until the end of the experiment. In flow-through experiments, fresh solution is fed continuously into the reactor and the reacted phases are collected continuously. The saturation state of the solution, which varies between flow-through and batch experiments, influences the reaction. Consideration must be given to whether the dissolution takes place under equilibrium or far from equilibrium conditions. In any experimental setup, accessory minerals can hardly be avoided and may have non-neglectable impact if they are dissolved and affect the overall dissolution.

Previous Studies on Dissolution of Raw and Calcined Clay Minerals in Alkaline Solutions

Many studies concentrated on the dissolution of various clays and clay minerals and calcined clays or clay minerals under alkaline conditions (Table 1). Due to the different approaches in the research areas, the experimental conditions differed significantly, e.g. in concentrations and types of alkaline solution, reaction times, and temperatures. For kaolinite and metakaolinite, congruent dissolution was observed up to concentrations of 4 mol/L NaOH or KOH. Dioctahedral smectites and metasmectites showed mainly incongruent dissolution in concentrations up to 5 mol/L of the alkaline activator solution. At a calcination temperature of 900°C a congruent dissolution for a metasmectite was observed, which was explained by the formation of a separate, inert SiO_2 phase at that temperature and, therefore, a reduction of dissolvable silica (Garg & Skibsted, 2015). Studies on illite and metaillite dissolution in alkaline activators with concentrations up to 6 mol/L showed a strong dependence of congruency on the calcination temperature. Uncalcined illite showed incongruent solubility, while for metaillite (calcined at <800°C) mostly congruent dissolution was observed.

While raw and calcined clay minerals in natural and geotechnical applications and even when used as supplementary cementitious materials (SCM) are subjected to pH <14, these materials react with NaOH of up to 18.94 mol/L (50%) when used as precursors for geopolymer binder production. As yet, the solubility characteristics in high molar alkaline solutions are not fully understood.

Additional silica or aluminum sources are regularly supplemented in geopolymer production. The aim is to adjust the Si:Al ratio of the evolving geopolymers, which can benefit the mechanical properties. For metakaolinite (with a natural Si:Al of 1:1), silica is used to increase the Si:Al. Metasmectite or metaillite have natural Si:Al ratios of 2:1 or higher, so aluminum can be used to decrease the ratio. Si:Al ratios in the broad range of 2:1–4:1 were mostly determined to be favorable.

The aim of the current study was to analyze the solubility of three different calcined clay minerals (metakaolinite, metamontmorillonite, and metaillite) in

Table 1 Summary of dissolution experiments in alkaline medium from prior studies

Material	Sample/ calcination (°C}	Si:Al	s/l	cNaOH (mol/L}	*T* (°C)	Congruent dissolution	Si:Al after reaction in solution	Reference
Bentonite (La Serrata, Spain)	Bulk/none	2.6	0.3	0.0001–0.5	35–90	No	3.4	Cuevas et al. (2006)
Bentonite (La Serrata, Spain)	Bulk/none	2.6	n.s.*	0.25	25–120	n.s.*	n.s.*	Fernández et al. (2006)
Boom clay (Belgium)	Bulk/none	n.s.*	0.25	0.1	60	No	6	Honty et al. (2010)
Bentonite (MX-80, USA)	Bulk/none	2.4	n.s.*	0.01, 0.3, 1	20	No	2.2	Karnland et al. (2007)
Opalinus clay	Bulk/none	n.s.*	0.02–0.2	0.01–0.1	150–200	n.s.*	n.s.*	Chermak (1992)
Kaolinite (from St. Austell, UK	<2 μm/none	1	0.004–0.01	KOH 0.1–4	35–80	Yes	1	Bauer et al. (1998)
Kaolinite (from Georgia, USA)	<1 μm/none	1	0.002–0.004	0.001, 0.01	25–60	Yes	1	Carroll-Webb & Walther (1988)
Kaolinite (KGa-1)	Bulk/none	1	0.002	0.001–0.1	25	Yes	1	Huertas et al. (1999)
Kaolinite (from St. Austell, UK)	<2 μm/none	1	0.004–0.01	KOH 0.1–4	35–80	Yes	1	Bauer & Berger (1998)
Smectite (from industrial bentonites)	<2 μm/none	2.4, 2.6	0.004–0.01	KOH 0.1–4	35–80	Yes	2.4, 2.6	Bauer & Berger (1998)
Smectite (from Cabo de Gata and Yunclillos deposits, Spain)	<2 μm/none	2.5	0.05	5	20	No	3.3	Elert et al. (2015)
Smectite (from natural bentonites)	Bulk/none	2.4	0.1	0.01	150	n.s.*	n.s.*	Mosser-Ruck & Cathelineau (2004)
Montmorillonite (from Cabo de Gata bentonite, Spain)	<4 μm/none	3	n.s.*	KOH 0.005–0-.5	50–70	No	3.3	Rozalen et al. (2009)
Montmorillonite (from MX-80, USA)	<2 μm/none	2.4	n.s.*	0.01, 0.3, 1	20	No	2.2	Karnland et al. (2007)
Montmorillonite (n.s*)	Bulk/none	n.s.*	0.005	1	90	n.s.*	2.9	Nakayama et al. (2004)
Illite (Illite de Puy)	<8 μm/none	2.1	n.s.*	0.03 and 0.05	5–50	No	1.8–3.3	Köhler et al. (2003)
Calcined kaolinite (KGa-2)	Bulk/500–900	1	0.00025	0.1	25	Yes	1	Garg & Skibsted (2019)
Calcined montmorillonite (SAz-2)	Bulk/500–900	2.5	0.00025	0.1	25	No	2.9–3.6	Garg & Skibsted (2019)
Calcined Illite (IMt-1)	Bulk/650–930	1.8	0.02	0.5	100	Yes	1.8	He et al. (1995a, b)
Calcined interstratified illite-smectite (natural clay)	Bulk/550–950	n.s.*	0.001	2.77	60	n.s.*	2.5	Buchwald et al. (2009)
Calcined interstratified illite-smectite (Friedland clay, Germany)	Bulk/850°C	2.3	0.001	6	25–75	No	3.1	Hu et al. (2017)
Calcined common clays (Belgium)	Bulk/700–900	1.45–4.1	0.0125	6	25	n.s.*	n.s.*	Khalifa et al. (2019)

*n.s. = not specified

high molar alkaline solution (NaOH), considering the influence of the preceding calcination and unavoidable mineral impurities. A further objective was to understand better the dissolution of an industrial crystalline aluminum hydroxide powder.

Materials and methods

Raw Materials

Three different clays were investigated. KBE-1, a Bavarian kaolin (Amberger Kaolinwerke Eduard Kick GmbH & Co. KG, Hirschau, Germany). Ceratosil® WG, a Bavarian bentonite (Clariant Produkte Deutschland GmbH, Frankfurt am Main, Germany), and Arginotec INX, an illitic clay (Arginotec GmbH & Co. KG, Huenxe, Germany).

The main mineral in KBE-1 was kaolinite (≥93 wt.%). The kaolinite is low *b*-axis error-ordered and consists of 46–47 mass% ordered kaolinite and 50–51 mass% disordered kaolinite. The disordered kaolinite is characterized by 93% BB/7% BC stacking sequences. 88% of BB sequences have no additional ~*b*/3 stacking errors (Izadifar et al., 2020). The Hinckley Index of the kaolinite was 1.63, characteristic of a well ordered kaolinite (Izadifar et al., 2020). Dioctahedral mica (muscovite), quartz, and anatase were present as accessory minerals (Table 2). The specific surface area of the bulk material was 9 m^2/g. KGa-2 (Georgia, USA) from the Source Clays Repository of The Clay Minerals Society was used as a second kaolinite for solubility experiments. The kaolinite content was 97.3 wt.% (Izadifar et al., 2020). KGa-2 showed 86% BB stacking sequences and a low abundance of BC stacking. The disorder was intermediate (Izadifar et al., 2020).

Ceratosil® WG consisted mainly of dioctahedral smectite (montmorillonite) with accessory silicates, cristobalite/opal-C, and carbonates (Table 2). The bulk material had a cation exchange capacity (CEC) of 81 cmol(+)/kg. Ca^{2+} accounted for the largest amount of the exchangeable cations (59%). Other exchanged cations were Mg^{2+} (21%), Na^{+} (17%), and K^{+} (3%). The montmorillonite was classified as a medium-charged *cis*-vacant montmorillonite (according to Emmerich et al., 2009) from composition and by dehydroxylation behavior (Drits et al., 1995; Wolters & Emmerich, 2007). The specific surface area was 58 m^2/g and, as the bentonite was similar to bentonite P in Delavernhe et al. (2015), its lateral dimension was ~101 nm. A second montmorillonite, which was the main component (96 wt.%) of bentonite Volclay (Wyoming bentonite, USA), was used for ancillary solubility experiments. The montmorillonite of Volclay was fully *cis*-vacant. The CEC was 85 cmol(+)/kg and interlayer occupation was Na^{+} (96.4%) and K^{+} (3.6%). The lateral layer dimension was ~277 nm (Delavernhe et al., 2015; Wolters et al., 2009). The BET surface was 39 m^2/g.

The dominant clay mineral in Arginotec INX was a dioctahedral *trans*-vacant interlayer-deficient mica ($2M_1$ polytype with its specific peaks in X-ray diffraction patterns; see Grathoff and Moore (1996) for distinction of illite polytypes). Arginotec INX contained small amounts (≤10 wt.%) of other clay minerals (kaolinite and trioctahedral mica) and accessory silicates, quartz, carbonates, sulfates, and phosphates (Table 2). The specific surface area of the bulk material was 110 m^2/g.

The structural formulae for montmorillonite of Ceratosil® WG $Ca_{0.1}Na_{0.1}Mg_{0.01}$ $(Si_{3.96}$ $Al_{0.04})$ $(Al_{1.48}Fe_{0.09}Mg_{0.51})$ $O_{10}(OH)_2$ and for illite of Arginotec INX $K_{0.75}$ $(Si_{3.5}$ $Al_{0.5})$ $(Al_{1.25}Fe_{0.5}Mg_{0.25})$ $O_{10}(OH)_2$ were calculated (according to Stevens, 1946) from XRF data (Table 3). The initial Si:Al ratios were 1.09 for the bulk material of KBE-1, 1.0 for the kaolinite, 3.55 for the bulk material of Ceratosil WG, 2.6 for the montmorillonite, 1.91 for the bulk material of Arginotec INX, and 2.0 for the illite.

Table 2 Mineral phases (wt.%)

Phase	KBE-1	Ceratosil WG	Arginotec INX
Kaolinite	93 (± 0.5)	-	5.4 (± 0.2)
Montmorillonite	-	67.1 (± 0.4)	-
Dioctahedral illite	-	-	76.4 (± 0.6)
Dioctahedral mica	5.5 (± 0.5)	2.4 (± 0.1)	-
Biotite (Phlogopite)	-	-	7.8 (± 0.3)
Zeolite (Heulandite)	-	0.9 (± 0.1)	-
Quartz	1 (± 0.5)	-	0.4 (± 0.2)
Cristobalite/Opal-C	-	13.3 (± 0.1)	-
K-Feldspar	-	10.4 (± 0.1)	4.4 (± 0.3)
Plagioclase	-	4.1 (± 0.3)	1.1 (± 0.5)
Calcite	-	1.9 (± 0.1)	2.4 (± 0.2)
Anatase	< 0.5	-	-
Anhydrite	-	-	1.4 (± 0.1)
Apatite	-	-	0.7 (± 0.1)

Table 3 Oxide and element compositions (wt.%, normalized to ignited state)

	KBE-1	Ceratosil WG	Arginotec NX	Hydrafil®
SiO_2	54.12	71.1	52.43	-
Al_2O_3	43.93	17.71	24.28	99.5
Fe_2O_3	0.4	1.31	8.74	0.01
MnO	-	0.07	-	-
MgO	-	3.91	4.02	-
CaO	0.1	2.72	1.46	0.1
Na_2O	-	1.08	-	-
K_2O	-	1.92	6.82	-
TiO_2	-	0.18	0.88	-
Si	25.32	33.24	24.74	-
Al	23.27	9.37	12.97	58.87
Fe	0.28	0.91	6.17	0.01
Mn	-	0.05	-	-
Mg	0.06	2.36	2.45	-
Ca	0.09	1.94	1.05	0.07
Na	0.01	0.8	-	-
K	0.47	1.59	5.71	-
Ti	0.38	0.11	0.53	-
O	50.11	49.62	46.38	47.05

Hereafter, the terms KBE-1, Ceratosil WG, and Arginotec INX will be used when referring to the bulk material. The term 'calcined' will be prefixed for heated samples. For observations related to the (dehydroxylated) main clay mineral itself, the terms (meta)kaolinite, (meta)montmorillonite, and (meta)illite will be used.

Furthermore, an industrially produced crystalline aluminum hydroxide powder (Table 3) (Hydrafil®, HPF – The Minerals Engineers, Frechen, Germany) was analyzed. The $Al(OH)_3$ was supposed to be used to reduce the Si:Al ratio of solid geopolymer precursors. The solubility of an amorphous SiO_2 powder (Amosil®, HPF – The Minerals Engineers, Frechen, Germany) for increasing the Si:Al ratio in geopolymers was already investigated in a previous work (Werling et al., 2020).

Analytical Techniques

Cation exchange capacity (CEC) was determined by the modified Cu-trien method. 50 mg of the powdered sample was mixed with 10 mL deionized water and 5 mL of a 0.01 mol/L copper-triethylentetramine (Cu-trien) solution in 15 mL centrifuge tubes. After shaking the sample by hand briefly, it was placed on a shaking table for 3 h. After shaking, the sample was centrifuged at 4500 rpm (4347×*g*) for 10 min (Heraeus Multifuge 3 S-R, Thermo Heraeus, Thermo Fisher Scientific Inc., Waltham, Massachusetts, USA). The absorbance of the supernatants was measured with a UV-Vis spectrophotometer (Genesys 10 UV, Thermo Electron Corporation, Waltham, Massachusetts, USA) at a wavelength (λ) of 580 nm using polystyrene microcuvettes (path length 1 cm; Lab logistics Groups GmbH, Meckenheim, Germany). The concentration of Cu-trien of the supernatants was determined by a calibration curve. CEC [cmol(+)/kg] was calculated by the depletion of the supernatant due to the uptake of Cu-trien into the interlayers of the smectites.

Simultaneous thermal analysis (STA) was conducted using a Jupiter 449 (Netzsch, Selb, Germany) thermal analyzer coupled with a mass spectrometer (Quadrupol 409 Aeolos, Netzsch, Selb, Germany). Before analysis the samples were stored under ambient conditions (21°C, 50–60% R.H.). For the measurements, ~100 mg of the powdered raw materials was heated from 35 to 1000°C with a heating rate of 10°C/min in a Pt-Rh crucible with a loose lid. An empty crucible with lid served as the reference. The measurements were carried out under an atmosphere of synthetic air (50 mL/min, purge gas) and nitrogen (25 mL/min, protective gas). Prior to the dynamic heating, an isothermal segment of 10 min at 35°C was performed to ensure stabilization of the measurement atmosphere.

Inductively coupled plasma optical emission spectrometry (ICP-OES) was carried out using an Optima 8300DV instrument (PerkinElmer, Waltham, Massachusetts, USA). The measuring range of Si and Al concentrations in solution was 30 mg/L. Liquid samples were acidified and diluted accordingly.

For X-ray diffraction (XRD) a Bruker D8 Advance A25 diffractometer (Bruker Corporation, Billerica, Massachusetts, USA) with a LYNXEYE XE Detector (2.94° opening angle) was used. Powdered samples (ground with a McCrone mill, <20 μm) were analyzed between 5 and 80°2θ. The step size was 0.02°2θ and the scan rate was 2 s per step. An automatic slit (primary side), soller collimators of 2.5° (primary and secondary side), and an automatic knife edge were used. The CuKα radiation (1.54 Å) was generated at 40 kV and 35 mA. For quantitative analysis, Rietveld software Profex

(Doebelin & Kleeberg, 2015; www.profex-xrd.org) was used.

Investigations with the environmental scanning electron microscope (ESEM) were performed with a Philips XL 30 environmental scanning electron microscope (Thermo Fisher Scientific Inc., Waltham, Massachusetts, USA). For ESEM micrographs, 2–3 mg/cm^2 of the powders of the raw clay samples, metaclay samples, and the dried residues were scattered on the sample holders. The powdered samples were investigated after applying a 5 nm coating of platinum. A scan throughout the complete sample holder was made to ensure homogeneous distribution of the sample. Subsequently, several sections were chosen for particle-size estimation.

Atomic force microscopy (AFM) for determination of the height of particles was carried out using a Bruker Dimension Icon (Bruker Corporation, Billerica, Massachusetts, USA). A grid of 1 μm×1 μm was investigated. A cantilever type MikroMasch (HQ:NSC15 AL/Bs: 320 kHz; 40 N/m) was used (MikroMasch, Tallinn, Estonia). A dispersion of 50 mg/L for each sample in ethanol (99.9%) was prepared. The dispersions were ultrasonicated (37 kHz) for 15 min. Subsequently, the dispersions were deposited on silica wafers by spin coating (WS-650MZ-23NPP, Laurell Technologies Corporation, North Wales, Pennsylvania, USA) at 2000 rpm. Spin coating was performed twice (~0.5 mL each time) to ensure a sufficient coverage with sample material.

The specific surface area was determined by Argon adsorption measurements at 87 K with a Quantachrome Autosorb 1-MP (Anton Paar GmbH, Ostfildern, Germany). The specific surface area was calculated with the Quantachrome program *ASiQwin 4.0*, according to the BET method on the raw and the calcined bulk materials (Brunauer et al., 1938). Before adsorption measurements, the powdered samples were outgassed at 95°C for 24 h in vacuum.

Experimental Procedure

Calcination of Clay Minerals

The calcination process to produce metaclay minerals was carried out in a L9/12/B180 furnace in air (Nabertherm GmbH, Lilienthal, Germany) with a heating rate of 10°C/min. 5 g of raw clay was heated in unglazed ceramic crucibles to the final temperature and immediately placed in a desiccator for cooling to room temperature. The calcination temperatures were selected based on STA results (Fig. 1). Kaolinite was calcined at 480, 555, 615, 700, and 900°C (Werling et al., 2020). For montmorillonite, calcination temperatures of 550, 670, 750, and 900°C (starting at the onset of dehydroxylation (DHX) and ending prior to recrystallization) were selected. The same criteria were applied to select the calcination temperatures for illite (300, 510, 650, 750, and 900°C). After calcination, all samples were stored in a desiccator until the preparation of the solubility experiments.

Determination of Dissolution Characteristics

The powdered (calcined) samples (0.1 g) were mixed with NaOH solution (5 g) in 50 mL polypropylene centrifuge tubes. This corresponded to a solid/liquid (s/l) ratio of 0.02. Concentrations of NaOH solutions were 0.01 to 10.79 mol/L, reflecting a pH value ranging between 12 and 14.73 (Table 4). The activity represents the effective molarity of the solutions. It can be calculated by multiplication of activity coefficient and molarity of the solution. For NaOH concentrations higher than 1 mol/L, activity coefficients increase (Table 4).

The reaction time for the solubility experiments was 24 h or 7 days, during which the samples were placed horizontally on a shaking table (Edmund Buehler GmbH, Bodelshausen, Germany). Subsequently, the samples were centrifuged (Heraeus Multifuge 3 S-R, Thermo Heraeus, Thermo Fisher Scientific Inc., Waltham, Massachusetts, USA) for 25 min at 4500 rpm (4347×*g*). The supernatant was decanted and 0.5 mL were acidified (with 7.5 mL of 1 mol/L HNO_3) and diluted (with 17 mL deionized water). Subsequently, 2.5 mL of the diluted solution were diluted again with 7.5 mL of deionized water (final dilution factor 1:200) for ICP-OES measurement.

The solid residuals were washed several times until the pH was equal to the deionized water used for washing (pH = 5.5). Afterwards, the samples were dried at room temperature and ground gently before the measurements to determine the morphology (SEM) and the phase content (XRD).

Differentiation between Silica Polymorphs

In bentonites, opaline silica polymorphs (opal-C and opal-CT) can be mistaken easily for cristobalite. Silica polymorphs such as opal-C and opal-CT show

Table 4 NaOH solutions

Molarity	(mol/L)	0.01	0.1	1	4	5	6.1	7.96	10.79
Concentration	(%)	0.038	0.38	3.8	13.9	16.88	20	25	32
pH	-	12	13	14	14.55	14.6	14.63	14.68	14.73
Molality	(mol/kg)	0.01	0.1	0.99	3.5	4	5	6	8
Activity coefficient*	-	-	0.777	0.668	-	0.900	1.065	1.287	1.992
Activity	(mol/L)	0.01	0.08	0.668	-	4.5	6.5	10.3	21.5

*Pabalan & Pitzer (1987)

reflections in XRD patterns near those of cristobalite. For opal-C a sharp reflection with a FWHM in a range of 0.222–0.453 Å would appear. Opal-CT shows a broader reflection with a FWHM ranging from 0.506–0.883 Å (Elzea et al., 1994). To differentiate between opal-C, opal-CT, and cristobalite the bulk sample was heated at 1050°C for 24 h (Elzea et al., 1994). The change of the d_{101} reflection near 4.0 Å in the XRD pattern indicates the nature of the silica polymorph. As opal-C and opal-CT are hydrated, the d_{101} reflection shifts and sharpens due to heating. Cristobalite does not change the position of its reflection (Elzea et al., 1994).

For quantitative analysis of the mixture of cristobalite and an opaline silica polymorph, the raw bulk material of Ceratosil WG was treated in boiling 0.5 mol/L NaOH for 10 min (Hillier & Lumsdon, 2008). By comparing the sample weight before and after dissolution, the silica polymorph and cristobalite could be quantified.

Results and Discussion

The thermal behavior of kaolinite for calcination as a geopolymer precursor was investigated in preliminary experiments (Werling et al., 2020). Only a small mass loss of 0.32% occurred up to 300°C due to dehydration. The DHX reached its peak (in the DSC curve) at 576°C and led to a weight loss of 13.04%. Recrystallization of the material started at 980°C (Fig. 2).

Thermal Behavior of Montmorillonite and Illite

The air-dry montmorillonite showed a mass loss of 11.11% caused by dehydration (DHD) with a peak temperature in the DSC curve of 151°C. The moisture content was obtained by adding the mass loss during the isothermal heating (100% minus starting mass of the dynamic measurement) to the mass loss during DHD. The moisture of this montmorillonite was 11.60%. A mass loss of 2.96% due to DHX occurred with the peak of the reaction (in the DSC curve) at 663°C (Fig. 1), which agreed with the DHX of mainly *cis*-vacant montmorillonites between 650 and 700°C (Emmerich et al., 2009). Normalized to the dry weight (after loss of moisture), the mass loss for DHX was 3.35%. This result confirmed the quantified amount of montmorillonite (67.1 wt.%) together with traces of mica. The DHX overlapped with the decomposition of calcite, which led to a further mass loss of 0.58% (normalized 0.66%). The mass loss corresponded to a calcite amount of 1.5 wt.%, the quantified amount of calcite was 1.9 wt.%. The deviation was probably caused by challenges in the determination of the mass loss values due to the overlap of the signals from H_2O and CO_2 loss. Recrystallization started at 990°C.

The mass loss (3.48%) of illite during DHD with a peak maximum in the DSC curve at 98°C was considerably smaller than for montmorillonite (Fig. 1). The moisture was 4.41%. During DHX a mass loss of 4.51% was observed with the peak maximum (in the DSC curve) at 504°C, which was characteristic for *trans*-vacant dioctahedral illite (Emmerich et al., 2009). Normalized to the dry weight the mass loss for DHX was 4.72%, which confirmed the quantified amount of illite in combination with the DHX of the quantified amount of kaolinite. The sample contained a small amount of calcite, which decomposed at 678°C with an associated mass loss of 1.10%. The normalized mass loss of 1.15% agreed with a calcite content of 2.6%, which was within the error of the quantification (2.4 ± 0.2 wt.%).

Phase Content of the Calcined Materials

The XRD patterns of KBE-1 with a calcination temperature of 480°C showed no changes compared to the raw material (for patterns see Supplementary Data). At

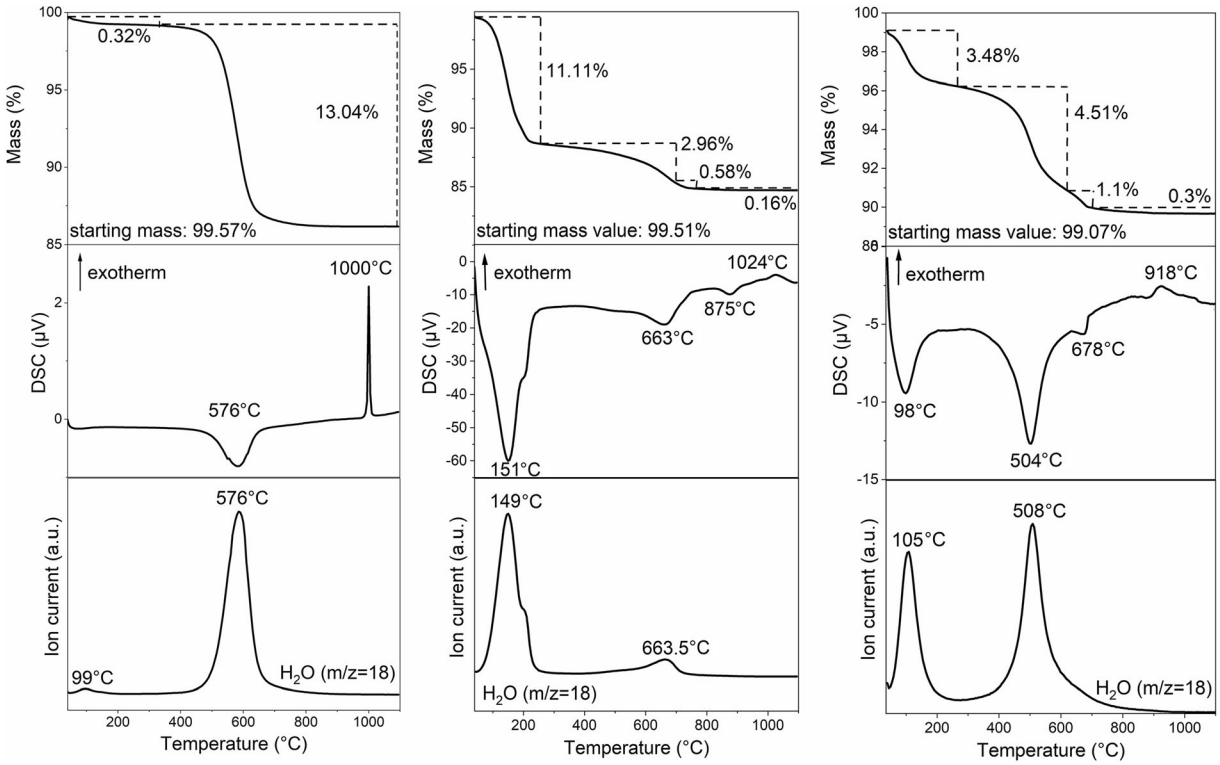

Fig. 1 Thermal behavior of kaolinite (left) from Werling et al. (2020), montmorillonite (middle), and illite (right)

555°C the background increased due to the formation of an amorphous phase. Kaolinite was still detectable, but the intensity of the peaks decreased. At 615°C kaolinite was completely transformed into amorphous metakaolinite. The broad hump between 15 and 30°2θ in the X-ray pattern due to an amorphous phase increased in intensity by calcination to 700°C. Kaolinite was already converted into amorphous metakaolinite before; therefore, only the accessories (mica, anatase, and quartz) were still detectable by XRD. The XRD pattern of the material did not change by calcination up to 900°C. At temperatures of ~1000°C, recrystallization of a defect spinel followed by mullite formation at ~1400°C would take place (Glass, 1954; Sonuparlak et al., 1987).

At a calcination temperature of 550°C for Ceratosil WG the reflections of montmorillonite were still detectable. Only the d_{001} reflection shifted to higher °2θ values due to dehydration of adsorbed water, which was completed at that calcination temperature. At 670°C the intensity of the montmorillonite reflections decreased. Calcite started to decompose. Further calcination to 750°C led to a further decrease in the intensity of the montmorillonite reflections. The accessories did not react, except calcite was decomposed completely and lime (CaO) was formed. The background increased, which indicated the formation of amorphous phases. At 900°C the reflections of montmorillonite were no longer detectable by XRD. No high-temperature phases were observed.

At a calcination temperature of 300°C for Arginotec NX, no changes compared to raw illite occurred. At 510°C the kaolinite reflections were reduced in intensity due to the start of the conversion into amorphous metakaolinite. At 650°C no kaolinite reflections were detectable anymore, which indicated that the total amount of kaolinite was transformed into metakaolinite. The d_{001} of illite was reduced slightly in intensity at that calcination temperature. The decomposition of calcite started, but small amounts of calcite were still detectable. For calcination at 750°C only slight differences (increase in background) could be observed. Metaillite still displayed similar reflections as illite. Phlogopite was not yet dehydroxylated at that temperature. DHX of phlogopites starts at >800°C. Therefore, the only layer silicate from which reflections disappeared was kaolinite due to the formation of amorphous metakaolinite. Phosphates, sulfates, quartz, and

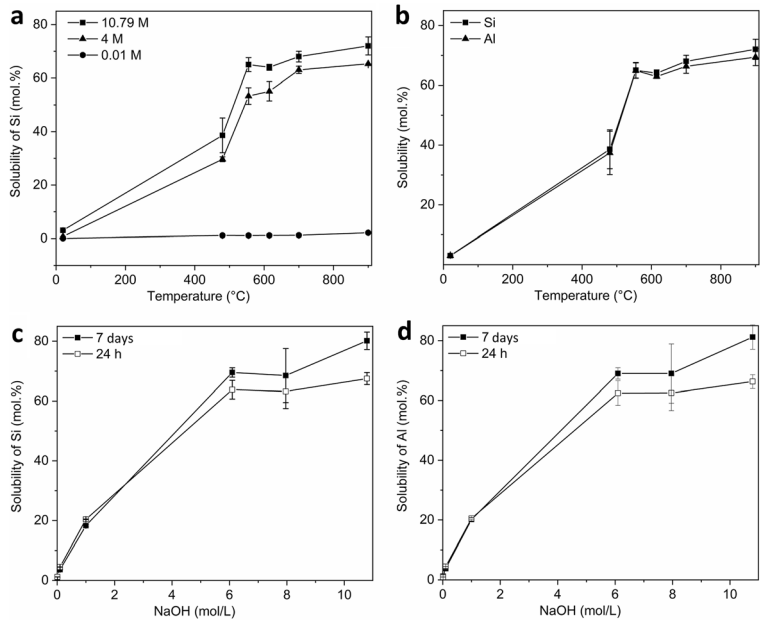

Fig. 2 **a** Solubility of Si (equal for Al) of metakaolinite in NaOH (10.79 mol/L, 4 mol/L, 0.01 mol/L) as a function of calcination temperature (reaction time 24 h) (from Werling et al., 2020). **b** Solubility of Si and Al of metakaolinite (reaction time 24 h, NaOH 10.79 mol/L). **c** Solubility of Si of metakaolinite as a function of NaOH concentration (reaction time 24 h and 7 days, calcination temperature 700°C) (from Werling et al., 2020). **d** Solubility of Al of metakaolinite as a function of NaOH concentration (reaction time 24 h and 7 days, calcination temperature 700°C)

feldspars did not change. During heating, α-quartz was transformed into β-quartz at 573°C, but after cooling of the sample, α-quartz was the existing phase again. Calcite was completely decomposed at 750°C at the expense of CaO formation. By calcination at 900°C the illite reflections decreased in intensity but were still detectable. No high-temperature phases formed.

Solubility of Clay Minerals

The metakaolinite showed congruent dissolution (Werling et al., 2020). The maximum solubility for the bulk material was reached in 10.79 mol/L NaOH (up to 70 mol.% of Si or Al after 24 h). This corresponded to a solubility of 77 mol.% of the metakaolinite after 24 h. It was increased at longer reaction times up to 80 mol.% of Si and Al of the bulk material after 7 days (Fig. 2a–d), which corresponded to a dissolution of 88% of the metakaolinite, while dissolution of the mica could be ignored. Mica did not contribute significantly to dissolution because it was not yet dehydroxylated during calcination of kaolinite. Assuming that mica (5.5 wt.%) showed a similarly low solubility as the undehydroxylated illite (max. 6 mol.%) studied here, a maximum contribution of 0.4% of mica to the total solubility of the material would be possible.

The first experiments on the solubility of a second kaolinite (KGa-2 (Georgia, USA) from the Source Clays Repository of The Clay Minerals Society; see Supplementary Data) indicated that the specific surface area of the material influenced the dissolution. The solubility experiments were performed according to the same procedure. Kaolinite was the main mineral of KGa-2 with 97.3 wt.% (Izadifar et al., 2020). Only small amounts of mica were present (0.5 wt.%). KGa-2 showed a high degree of structural disorder and had a significantly lower Hinckley Index (0.5) compared to KBE-1 (Izadifar et al., 2020). The DHX was comparable to KBE-1 and the DHX peak temperature was in the range of 20°C (Izadifar et al., 2020). Compared to KBE-1 the particle size of KGa-2 was smaller. KGa-2 had a larger BET surface of 18 m^2/g compared to KBE-1. The maximum solubility of KGa-2 for the metakaolinite (at calcination temperatures of 540, 615, and 700°C) was 86 mol.% Si and 84 mol.% Al in 10.79 mol/L NaOH already after 24 h. Due to particles with a larger specific surface area, the dissolution seemed to be accelerated. But, the influence of disorder and particle size/surface area on dissolution were not clearly distinguishable.

Solubility of Montmorillonite and Metamontmorillonite

The amounts of dissolved Si and Al measured by ICP-OES were used to calculate the solubility of (meta)montmorillonite (for total dissolved values see Supplementary Data). The raw material and the material calcined at 900°C showed the lowest solubility for metamontmorillonite after 24 h in any concentration of

NaOH (Fig. 3a). Thereby, the dissolved Si (7.8 mol.%) from metamontmorillonite calcined at 900°C was even lower than the dissolved Si (24.6 mol.%) from the raw montmorillonite in 10.79 mol/L NaOH. Otherwise, the solubility of the metamontmorillonite increased with increasing the calcination temperature up to 63.5 mol.% after calcination at 750°C in 10.79 mol/L NaOH (Fig. 3a). Dissolution of the raw montmorillonite as well as the metamontmorillonite increased with NaOH concentration from 0.01 to 10.79 mol/L. In 0.01 mol/L NaOH a maximum of 0.4 mol.% Si (for calcination temperatures of 670 and 750°C) was dissolved. At 4 mol/L NaOH the solubility of Si rose to a maximum of 42.6 mol.% (at a calcination temperature of 750°C). Due to simplicity of presentation not all of the analyzed NaOH concentrations are shown in the figures (for remaining concentrations see Supplementary Data).

Both montmorillonite and metamontmorillonite showed an incongruent dissolution of Si and Al (Fig. 3b), which was also observed at low NaOH concentrations by Bauer and Velde (1999) and by Garg and Skibsted (2015). Garg and Skibsted (2015) as well as Khalifa et al. (2020) suggested that Si dissolves faster from the structure than Al at low NaOH concentrations, as in the distorted 2:1 layers of metamontmorillonite Al hexahedra are enclosed by Si tetrahedra.

Nevertheless, the solubility of Al in metamontmorillonite increased with increasing concentration of NaOH. The highest solubility for Al of the metamontmorillonite (42.1 mol.%) was reached in 10.79 mol/L NaOH for a calcination temperature of 750°C. Calcination temperatures significantly greater than DHX can lead to the formation of segregated SiO_2 and crystalline silicates (Grim & Kulbicki, 1961), which are less soluble. This changes the Si:Al in the still soluble phases of the metamontmorillonite and can lead to reduced leaching of Si and, therefore, apparent congruent dissolution of metamontmorillonite. However, X-ray diffraction of the material calcined at 900°C did not show newly formed crystalline silicates. The reduction of the solubility could be explained by sintering of metamontmorillonite. Due to the formation of large particles (and the reduction of specific surface area), particles within the agglomerates were less accessible for the alkaline activator solution and, therefore, the amounts of dissolved Si and Al decreased (Dietel et al., 2017).

In subsequent experiments the reaction time was increased to 7 days, to determine whether the reaction was completed after 24 h. The samples with a calcination temperature of 750°C, which showed the greatest solubility after 24 h, were leached in the different NaOH concentrations (Fig. 3c). The maximum solubility for metamontmorillonite was increased by 20.6 mol.% up to 84.1 mol.% Si at a reaction time of 7 days. For Al the increase in solubility after 7 days was even higher (25.8 mol.%), a maximum of 67.9 mol.% Al was reached (Fig. 3d). The Si:Al ratio (in solution) for the metamontmorillonite in the different NaOH concentrations ranged from 1.6–3.0 after 24 h, and from 1.2–2.1 after 7 days. The Si:Al ratios showed that the dissolution was more incongruent after 24 h compared to dissolution after 7 days.

To determine the dissolved Si from metamontmorillonite, the amount of dissolved Si from the accessory minerals must be considered, especially in the case of the nature of the accessory SiO_2 in Ceratosil WG, the solubility of which plays an important role. The FWHM of the d_{101} reflection of 0.309 was in the range of that for opal-C (0.222–0.453; Elzea et al., 1994). After heating, the reflection sharpened (see Supplementary Data for XRD pattern) and the FWHM decreased to 0.208. The mass loss of the sample due to the dissolution procedure (Hillier & Lumsdon, 2008) indicated that Cerastosil WG contained 54% opal-C and 46% cristobalite. The total solubility of Si was, therefore, increased by the simultaneous dissolution of opal-C with metamontmorillonite. While cristobalite is considered to be essentially insoluble (Hillier & Lumsdon, 2008) the amount of total dissolved Si from raw and calcined Ceratosil WG was increased by 10.1 mol.% due to opal-C dissolution. The total SiO_2 in Ceratosil WG was 71.1 wt.%. Ceratosil WG contained 13.3 wt.% silica polymorphs. Therefore, the silica polymorphs accounted for 18.7% of the total SiO_2 and the montmorillonite accounted for 64.3%. The remaining SiO_2 originated from the accessory silicates. 54% of the silica polymorphs was soluble opal-C, 46% was insoluble cristobalite. Accordingly, opal-C accounted for 10.1% of total SiO_2 and cristobalite for 8.6%.

Even though, from studies about pozzolanic reactions, small amounts of cristobalite are believed to be dissolved due to pH increase from lime hydration after longer reaction times (>5 days; De Windt et al., 2014), the amount of dissolved crystalline cristobalite in the present study was considered to be low after 24 h reaction time. As cristobalite was still detectable by XRD of the residue after the alkaline treatment, only small

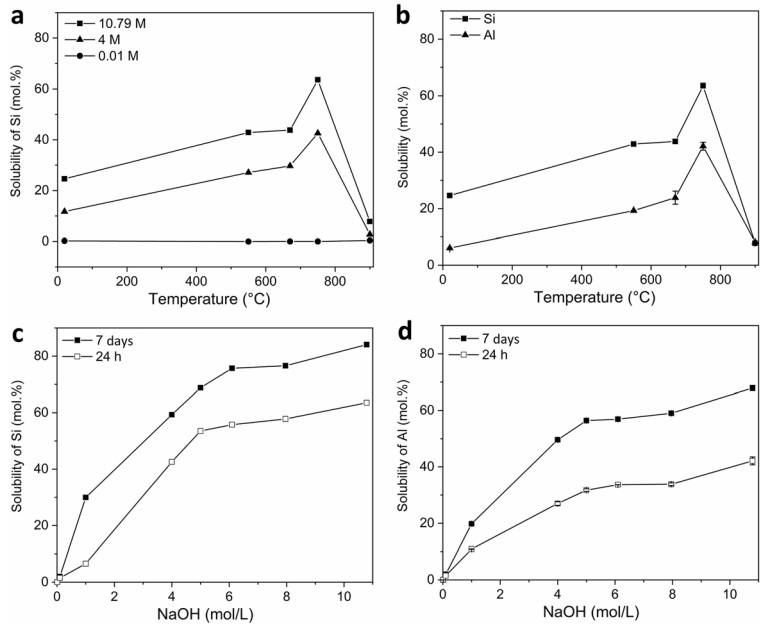

Fig. 3 **a** Solubility of Si of metamontmorillonite in NaOH (10.79 mol/L, 4 mol/L, 0.01 mol/L) as a function of calcination temperature (reaction time 24 h). **b** Solubility of Si and Al of metamontmorillonite (reaction time 24 h, NaOH 10.79 mol/L). **c** Solubility of Si of metamontmorillonite as a function of NaOH concentration (reaction time 24 h and 7 days, calcination temperature 750°C). **d** Solubility of Al of metamontmorillonite as a function of NaOH concentration (reaction time 24 h and 7 days, calcination temperature 750°C)

amounts of cristobalite could have been dissolved even after 7 days reaction time. Further contributions to Si and Al solubility for calcined Ceratosil WG from heulandite and feldspars were neglected. Heulandite showed a solubility of 4 mol.% for Si and 6 mol.% for Al in 10 mol/L NaOH (s/l = 0.025) after 5 h (Xu & van Deventer, 2000), and the solubility for the plagioclase was <4 mol.% for Si and Al in the same study. Solubilities between 0.15% (0.07% Si) and 0.32% (0.17% Al) of the total SiO_2 and Al_2O_3 was calculated from the data of solubility experiments for feldspars by Locati et al. (2010) in 1 mol./L NaOH for 24 h at 80°C. As only <1 wt.% heulandite was present in Ceratosil WG, the amount of this accessory dissolved was ignored; the contribution from feldspar dissolution was also ignored even though the amount of feldspar in Ceratosil WG was greater than the zeolite content.

As for kaolinite, complementary solubility experiments with a second montmorillonite (Volclay – Wyoming bentonite, USA; Wolters et al., 2009) were conducted first (see Supplementary Data; bulk material was used for experiments). Montmorillonite of Volclay is completely *cis*-vacant, unlike Ceratosil WG. Furthermore, the particle size of montmorillonite from Volclay was significantly larger (Delavernhe et al., 2015) and, thus, the BET surface area was smaller than for the montmorillonite of Ceratosil WG described here. The first results indicated that the larger particles of Volclay showed a significantly smaller solubility due to smaller amount of edge surfaces, which matched observations for the influence of specific surface area on solubility of the metakaolinites; but, distinguishing between the influence of particle size/surface area and location of the vacancy on the dissolution was not possible. Volclay showed a maximum solubility for metamontmorillonite of 14.5 mol.% Si and 10.5 mol.% Al after 24 h (for calcination temperatures of 710 and 800°C) in 10.79 mol/L NaOH. As for the preliminary metamontmorillonite described, the solubility was incongruent. The solubility decreased significantly at a calcination temperature of 930°C (max. 2 mol.% Si). After 24 h, both metamontmorillonites showed a ratio of dissolved Si and Al > 1.4 (1.4 for Volclay and 1.5 for Ceratosil WG). The ratio of dissolved Si and Al of Ceratosil WG after 7 days decreased to 1.2; a similar trend would be expected for Volclay at longer reaction times.

Solubility of Illite and Metaillite

As for (meta)montmorillonite, the amounts of dissolved Si and Al measured by ICP-OES were used to calculate the solubility of (meta)illite (for total dissolved values see Supplementary Data). After 24 h the lowest solubility was reached by the raw illite, e.g. 6 mol.% Si in

10.79 mol/L NaOH (Fig. 4a). The illite calcined at 300°C showed a comparably low dissolution (7 mol.% Si in 10.79 mol/L NaOH), due to the fact that the DHX just started at that temperature and, therefore, the reactivity was not yet elevated. The solubility of (meta)illite increased with increasing calcination temperature (510°C < 650°C < 750°C) and with increasing NaOH concentration. In 0.01 mol/L NaOH the solubility of Si did not exceed 2.5 mol.% regardless of the calcination temperature. The greatest solubility for metaillite of 44 mol.% Si was reached at a calcination temperature of 750°C in 10.79 mol/L NaOH. The maximum amount of dissolved Al was 42 mol.% in 10.79 mol/L at a calcination temperature of 750°C. The solubility of Al increased with calcination temperature and concentration of NaOH comparable to solubility of Si. The XRD pattern of the material calcined at 900°C did not provide an explanation for the decreased solubility. No newly formed high-temperature phases could be detected. The reduction in solubility may have been caused by sintering of metaillite, which was observed by others previously (Buchwald et al., 2009; Dietel et al., 2017; He et al., 1995a, b).

The solubility of Al and Si of metaillite (750°C) seemed to be congruent within a deviation of max. 2 mol.% (Fig. 4b). Previous studies showed a strong dependence on calcination temperatures for congruency of dissolution of Si and Al from illite in 0.03–2.77 mol/L NaOH (He et al., 1995a, b; Köhler et al., 2003; Seiffarth et al., 2013). Uncalcined illite materials showed incongruent solubility behavior (He et al., 1995a, b; Köhler et al., 2003). For calcined illite, the method and temperature of calcination had a clear influence on solubility. For a common clay, mainly consisting of illite (37.8 wt.%) and quartz (36.8 wt.%), calcination under a reducing atmosphere led to congruent and higher solubilities, but calcination temperatures >800°C led to incongruent dissolution independent of calcination atmosphere (Seiffarth et al., 2013). For standard illite IMt-1 the solubility was incongruent for the raw material and calcination temperatures >800°C. Calcination between 650 and 790°C led to a congruent dissolution (He et al., 1995a, b).

As for metamontmorillonite, the reaction time was increased for metaillite from 24 h to 7 days (Fig. 4c). The metaillite calcined at 750°C was chosen for these experiments due to the highest solubility after 24 h. The increase of solubility of metaillite was comparable to the observations for metamontmorillonite. The maximum solubility of Si increased up to 62 mol.% in 10.79 mol/L NaOH. The solubility of Al reached 56 mol.% (Fig. 4d).

The phlogopite of Arginotec INX was not dehydroxylated at the calcination temperature of 750°C. Therefore, the reactivity of the phlogopite was assumed to be low and dissolution could be ignored, whereas the kaolinite was fully transformed into

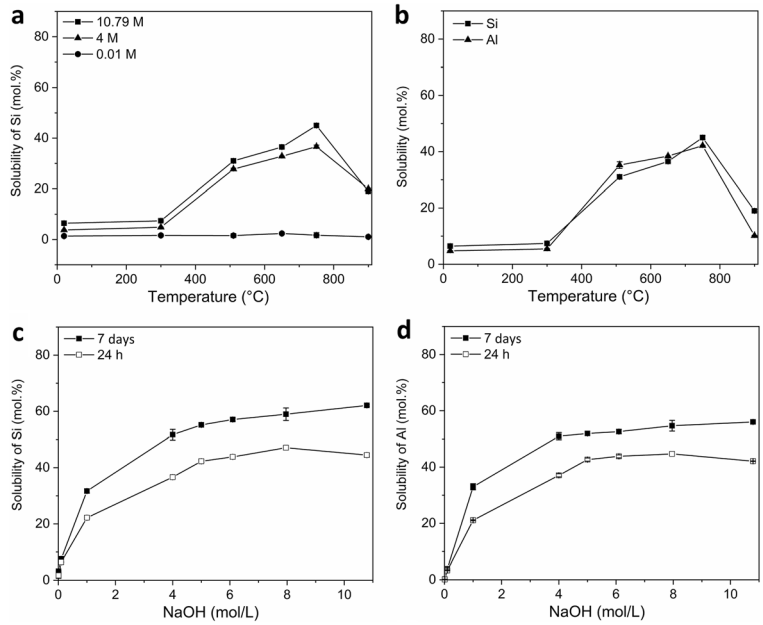

Fig. 4 **a** Solubility of Si of metaillite in NaOH (10.79 mol/L, 4 mol/L, 0.01 mol/L) as a function of calcination temperature (reaction time 24 h). **b** Solubility of Si and Al of metaillite (reaction time 24 h, NaOH 10.79 mol/L). **c** Solubility of Si of metaillite as a function of NaOH concentration (reaction time 24 h and 7 days, calcination temperature 750°C). **d** Solubility of Al of metaillite as a function of NaOH concentration (reaction time 24 h and 7 days, calcination temperature 750°C)

metakaolinite and, therefore, dissolved simultaneously with metaillite. The amount of Si and Al dissolved from metakaolinite contained in calcined Argiontec NX increased the total dissolved Si by a maximum of 5 mol.% and the total dissolved Al by 10 mol.% (for total dissolved values see Supplementary Data).

As Arginotec NX contained <6 wt.% feldspars, the assumption was that the contribution to the total solubility could be ignored.

For investigations of the influence of the specific surface area on illite solubility, further experiments on illites with different particle sizes will be necessary. The results will almost certainly be similar to the observations made for metakaolinite and metamontmorillonite.

Illite and montmorillonite showed different DHX temperatures, but anhydrous structures were still detectable by XRD after calcination. Both minerals retained some of their crystal structure after DHX. The structure of montmorillonite was lost at temperatures >750°C, which was within the range of 700–800°C observed in former studies (McConville & Lee, 2005). Regardless of the DHX temperature, the structure of illite was not completely lost up to 900°C, only the reflection intensity in the X-ray pattern was decreased, due to the beginning of decomposition.

The trends of dissolution for all investigated clay minerals were comparable to the trends in previous studies, although the overall dissolution (in %) can scarcely be compared due to different concentrations and types of alkaline solutions (Table 1). The observations herein showed that the dissolution decreased in the order metakaolinite > metamontmorillonite > metaillite. As shown in previous studies, the dissolution of kaolinite was congruent. Dissolution of montmorillonite was incongruent and for illite congruency was dependent on calcination temperature. The difference in congruency could be triggered by the (5-times) higher Fe content of illite compared to montmorillonite, while Mg was (2-times) lower. A higher Fe content influences the dissolution positively, which could have led to the congruent solubility of illite compared to incongruent solubility of montmorillonite. The difference in total amount of solubility of the two 2:1 layer silicates could appear due to the turbostratic disorder of the montmorillonite. By this disorder the edge surfaces could be more accessible for the alkaline solution and, therefore, the dissolution of the montmorillonite would be increased.

Solubility of Aluminum Hydroxide and Amorphous SiO_2

The solubility of Hydrafil® after 24 h increased with the NaOH concentration (Fig. 5). In 0.01 mol/L NaOH the lowest solubility was determined (0.3 mol.%). The greatest solubility of Al after a reaction time of 24 h was reached in 10.79 mol/L NaOH with 89 mol.%. By increasing the reaction time to 7 days, the maximum solubility of 90 mol.% was reached using 6.1 and 7.96 mol/L NaOH, not only in 10.79 mol/L. Compared to the solubility of an amorphous SiO_2, which reached a solubility of 25 mol.% Si after 24 h and 55 mol.% after 7 days (Werling et al., 2020), the $Al(OH)_3$ dissolved to a greater extent. The different solubilities of SiO_2 and $Al(OH)_3$ have to be taken into account when used for adjustment of the Si:Al ratio.

The results were comparable with a solubility of 30% observed by Pereira et al. (2009) in 1.2–2.5 mol/L NaOH after 5 days for synthetic $Al(OH)_3$ (gibbsite). Thus, any $Al(OH)_3$ source could be used to adjust the Si:Al ratio in geopolymers while the solubility of even amorphous SiO_2 varies between natural and synthetic material.

Morphology, Microstructure, and Composition of Residues

Micrographs of the materials were taken before calcination, after calcination, and from the residues after the solubility experiments to show the changes in particle morphology and microstructure of the materials. The raw kaolinite displayed the structure of stacked plates (diameter 0.5–3 μm; height 80–200 nm) consisting of ~110–290 layers, characteristic for many kaolinites (Fig. 6a). After the calcination process, the plates in metakaolinite were reduced slightly in height to ~40–120 nm (Fig. 6b), but still observable. The specific surface area of the bulk material was still 10 m^2/g after calcination at 700°C. Metakaolinite, calcined at 700°C, was dissolved up to 80 mol.% (Al and Si) after 7 days' reaction time (Werling et al., 2020). The solid residues showed small spherical particles which were formed on the surface of larger agglomerates. At high resolution those particles appeared to have a morphology similar to hydrosodalite or nanosheets from FAU-type zeolites, but the spherical particles were X-ray amorphous (for diffraction patterns see Supplementary Data). Neither for the spherical particles nor for the agglomerates could

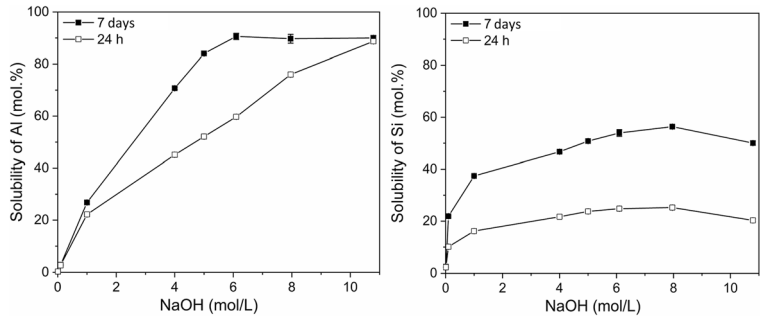

Fig. 5 Solubility of Al of $Al(OH)_3$ (left) and Si of amorphous SiO_2 (right, according to Werling et al., 2020) as a function of NaOH concentration (reaction time 24 h and 7 days)

a stacked platy structure be observed for the solid residual at lower resolution (Fig. 6d). Agglomeration of particles was visible at lower resolution. The agglomerates formed showed diameters up to 50–60 μm.

The raw montmorillonite showed aggregates (diameters between 4 and 11 μm) where single particles or stacks of layers could not be separated (Fig. 7a). During calcination the plates of the montmorillonite were fused together. The typical platy morphology got less obvious in the metamontmorillonite (Fig. 7b). The specific surface area decreased from 58 to 37 m^2/g after calcination at 750°C. It has to be noted that the BET surface was measured for the bulk material, not pure metamontmorillonite. The size of the aggregates did not change. Metamontmorillonite, calcined at 750°C, showed a solubility up to 84% Si and 68% Al after 7 days' reaction time. In the residue of the metamontmorillonite the platy structure was still observable for several grains (Fig. 7c). Agglomerates with diameters up to 75 μm existed (Fig. 7d). X-ray diffraction patterns (see Supplementary Data) showed small amounts of hydrotalcite ($Mg_6Al_2CO_3(OH)_{16}{\cdot}4H_2O$), which was precipitated as a new phase. After alkaline treatment reflections of metamontmorillonite were no longer detectable. One can assume that the hydrotalcite was formed of Al and Mg, which was dissolved from the metamontmorillonite, together with either airborne CO_2 or CO_3^{2+} released due to calcite dissolution.

In addition to the ESEM investigations, the raw montmorillonite and the metamontmorillonite calcined at 750°C were analyzed by AFM. Raw montmorillonite showed particle heights of between 2.7 and 3.8 nm. Primary particle diameters up to ~40 nm were considerably smaller than indicated by the supplier (≤30 μm, aggregates, secondary particle size). Primary particles were dispersed by the ultra-sonication process before AFM measurements, which destroyed aggregates in the material. The heights of the particles showed that delamination of the layers was not reached for this material. This was already assumed because Ceratosil WG contained Ca^+ as the interlayer cation, which strongly connected the layers and was responsible for preferred formation of aggregates. For Na-saturated montmorillonites, complete delamination was observed by others (Assemi et al., 2015; Delavernhe et al., 2015). Calcination at 750°C caused the particle heights to decrease to ~1.5 nm. The distribution of the particle diameters was also reduced slightly by calcination (~30 nm).

The raw illite (Fig. 8a) showed aggregates with diameters of 2–4 μm with particles of small diameters (40–250 nm). The particle size of metaillite hardly decreased during calcination (Fig. 8b) and the size of the aggregates was retained. The specific surface area of the bulk material decreased from 110 to 86 m^2/g after calcination at 750°C. Metaillite, calcined at 750°C, showed a solubility up to ~60% for Si and Al after 7 days' reaction time. The residue of the dissolution experiment showed agglomeration of smaller particles, but the platy structure was somehow retained (Fig. 8c). Thereby, agglomerates with diameters between 50 and 75 μm were formed (Fig. 8d). The reflections in the X-ray patterns similar to raw illite (see Supplementary Data) were still present. The phases contained in the residue were equivalent to the phases in the calcined material.

As for montmorillonite, AFM investigations were executed for the raw illite and metaillite (calcined at 750°C). Raw illite showed heights up to 2.9 nm, which was lower on average than the particles of the raw montmorillonite. The particle diameters were between 20 and 40 nm, while the D_{50} was determined with <150 nm by conventional particle-size measurements. Metaillite contained few larger aggregates (8.9–9.5 nm); but, except from those

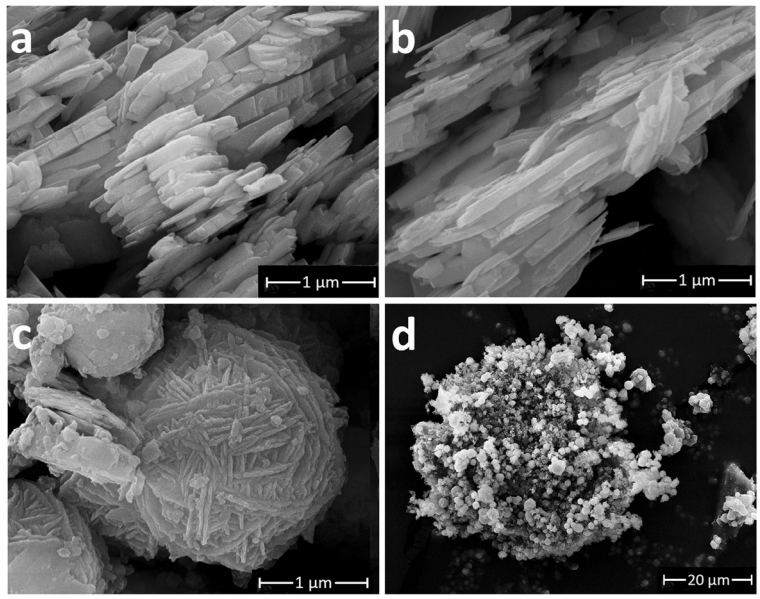

Fig. 6 **a** Raw kaolinite of KBE-1. **b** Metakaolinite (calcination temperature 700°C). **c** Solid residue of metakaolinite (calcination temperature 700°C) after alkaline treatment (NaOH 10.79 mol/L, reaction time 7 days). **d** Overview. Solid residue of metakaolinite (calcination temperature 700°C) after alkaline treatment (NaOH 10.79 mol/L, reaction time 7 days)

aggregates, the particle height was comparable to that of raw illite. A sample height of 0.9 nm would correspond to a single layer of illite.

The morphology of clay minerals has a significant influence on their solubility properties. A progressive decrease of the specific surface area at calcination temperatures (775–925°C) higher than the DHX temperature was observed for Friedland clay due to partial sintering of grains (Dietel et al., 2017). Friedland clay contains kaolinite as well as an interstratified illite-smectite. The decrease of the specific surface area (by one fifth) and, therefore, increase of particle size led to a decrease in the solubility (by about half) of Friedland clay in 5 mol/L KOH (Dietel et al., 2017). The same observations were made for samples of the same clay-mineral type (e.g. kaolinite group) described in this work. The calcined samples with a larger specific surface area showed an increased solubility. Still, metaillite solubility was considerably lower than the solubility for the other metaclay minerals, although the material showed the largest specific surface area. Therefore, the specific surface area can only be used to predict the solubility for the same type of clay mineral. Furthermore, this trend can only be observed for dehydroxylated clay minerals. The raw materials with larger specific surface areas showed considerably lower solubilities because of the reduced reactivity without preliminary DHX.

Suitability as Precursors for Geopolymers

The materials studied differed in the purity of the clay minerals. The chosen kaolin was relatively pure (93 wt.% kaolinite). The bentonite as source of montmorillonite (67.1 wt.% montmorillonite) showed larger amounts of impurities, such as 13.3 wt.% silica polymorphs, >10 wt.% feldspars, and 1.9 wt.% calcite. The studied illite (76.4 wt.%) had slightly smaller amounts of impurities compared to the montmorillonite but was not as pure as the kaolin. Therefore, the amounts of phases not contributing to the evolving geopolymer matrix would be different. The impurities with low solubility could function as fillers but the formation of different phases simultaneously with geopolymer formation could not be excluded. The phases formed during geopolymer production with the studied materials need to be investigated further.

For the metaillite studied, as with metamontmorillonite, the highest solubility for Si and Al was reached with a calcination temperature of 750°C in 10.79 mol/L NaOH although the dehydroxylation temperature (T_{DHX}) at 504°C of the *trans*-vacant illite in Arginotec IXN was much lower than T_{DHX} at 663°C for the *cis*-vacant montmorillonite of Ceratosil WG. Thus, 750°C was considered as the optimal calcination temperature for the thermal activation of these materials prior to the production of geopolymers. Earlier studies of Garg and Skibsted (2015) and Seiffarth et al. (2013)

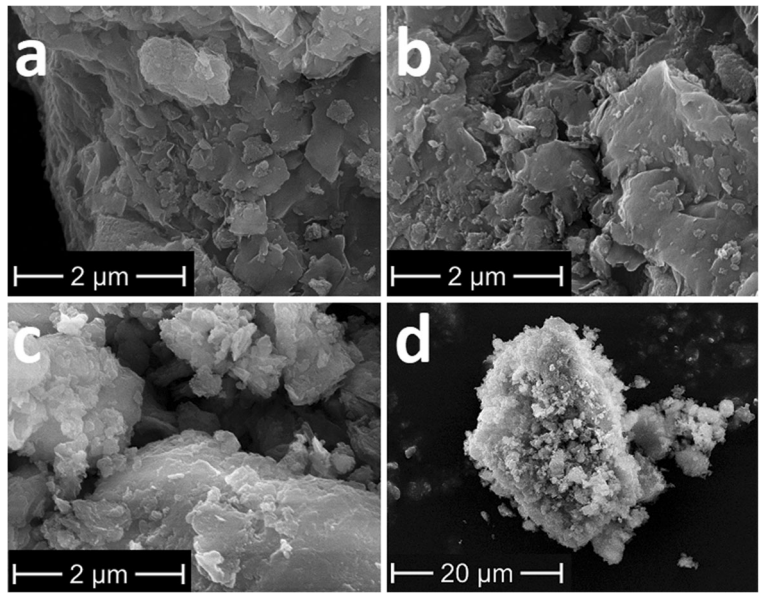

Fig. 7 **a** Raw montmorillonite of Ceratosil WG. **b** Metamontmorillonite (calcination temperature 750°C). **c** Solid residue of metamontmorillonite (calcination temperature 750°C) after alkaline treatment (NaOH 10.79 mol/L, reaction time 7 days). **d** Overview. Solid residue of metamontmorillonite (calcination temperature 750°C) after alkaline treatment (NaOH 10.79 mol/L, reaction time 7 days)

found optimal calcination temperatures of 800°C for two montmorillonites and between 750 and 800°C for an illite and an interstratified illite-smectite. The optimal calcination temperature for the well ordered kaolinite was slightly lower at 700°C.

The optimal calcination temperature determined in this study applies only for the clay minerals investigated here. General statements about the optimal calcination for kaolinites cannot be derived directly from these findings. For dioctahedral 2:1 layer silicates, e.g. montmorillonites and illites, taking into account the influence of octahedral vacancies on the dehydroxylation behavior will be necessary. As *trans*-vacant varieties dehydroxylate at much lower temperatures than *cis*-vacant varieties, the optimal calcination for *cis*-vacant might differ from that of *trans*-vacant varieties, although the present results indicate that the optimal calcination temperature was in the same range for both varieties. With an increasing number of studies about calcination, setting up general rules about optimal calcination temperatures for clay mineral groups may be possible in the future.

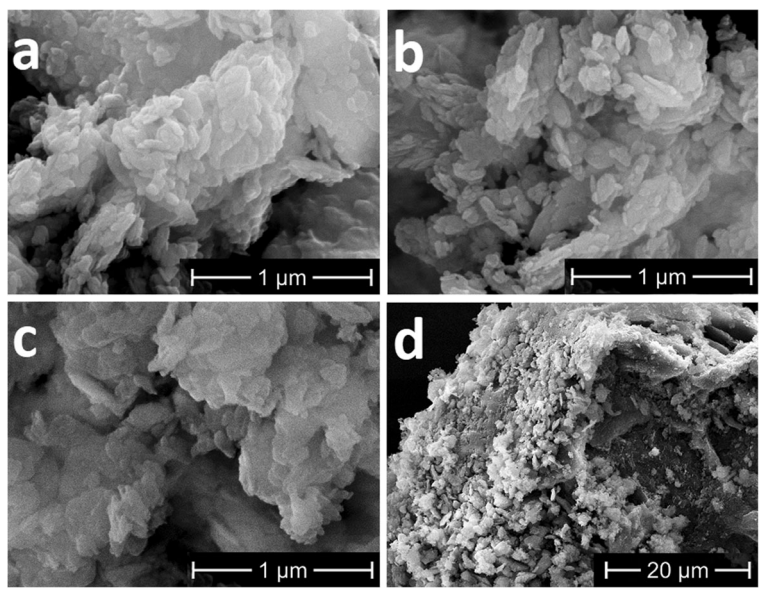

Fig. 8 **a** Raw illite of Arginotec NX. **b** Metaillite (calcination temperature 750°C). **c** Solid residue of metaillite (calcination temperature 750°C) after alkaline treatment (NaOH 10.79 mol/L, reaction time 7 days). **d** Overview. Solid residue of metaillite (calcination temperature 750°C) after alkaline treatment (NaOH 10.79 mol/L, reaction time = 7 days)

Thermal activation of all three clay minerals was regarded as successful, as >50% of the metaclay minerals was dissolved with the optimal thermal pretreatment. The production of geopolymers with those materials in water glass ($Na_{2x}Si_yO_{2y+x}$) free systems by sole activation with NaOH would be possible. The first tests producing geopolymers with varying Si:Al ratios, NaOH concentrations, and solid/liquid ratios, showed that geopolymers with a metakaolinite (Werling et al., 2020), metaillite, or metamontmorillonite precursor hardened. Further experiments on mechanical properties and phase content will follow. In the case of an adjustment of the Si:Al ratio with respect to Al, the solubility of Hydrafil® indicated that a pre-solution in NaOH would be useful if the geopolymers were produced with lower NaOH concentrations. For geopolymers produced with 10.79 mol/L NaOH, pre-solution would not yield any advantage. The influence of adjusting the Si:Al ratio needs to be studied further. Incomplete dissolution (<100%) for all studied clay minerals and $Al(OH)_3$ must be considered for the stoichiometric composition of the resulting geopolymers. By using more $Al(OH)_3$, the desired Si:Al could be reached, but simultaneously the amount of unreacted powder in the sample would increase. Depending on the material properties (e.g. particle size), unreacted $Al(OH)_3$ could act as a filler without negative impacts on the evolving geopolymers. Fillers can have a positive influence on the mechanical properties of the resulting geopolymer, e.g. by increasing compressive strength (Duxson et al., 2005; Xu & Van Deventer, 2000). Incomplete dissolution of the metaclay minerals can lead to excess Na^+ which does not react. Due to free Na^+, carbonation of the geopolymers can appear and affect the mechanical properties of the binder (Fletcher et al., 2005; Nikolov et al., 2017; Werling et al., 2020). Furthermore, for metamontmorillonite the incongruent dissolution led to smaller amounts of dissolved Al than expected. It has to be considered that the Si:Al ratio of a geopolymer produced with this metamontmorillonite will be lower than the stoichiometric ratio of the montmorillonite.

The dissolved Si from both the metamontmorillonite and opal-C could form CSH phases together with Ca from the metamontmorillonite and the decomposed calcite during geopolymer production (De Windt et al., 2014) or the Si:Al ratio of the emerged geopolymers would increase. CSH phases could coexist with the geopolymer matrix. Instead of the evolution of CSH phases, the formation of CASH or N(C)ASH may also be possible. Coexistence of NASH phases with calcium-containing phases is possible.

Generally, emphasis is necessary that the findings from solubility experiments are limited, given that the liquid:solid ratio differs from that used for geopolymer production; but, even during solubility experiments, reaching 100% solubility was not possible. Therefore, further studies will be necessary to answer satisfactorily whether this happens due to thermodynamic or kinetic effects.

Summary and Conclusions

The montmorillonite studied showed DHX at the highest temperature (663°C), kaolinite was intermediate (583°C), and illite was the lowest (504°C). Optimal thermal activation due to maximum dissolution was obtained at 700°C for the studied kaolinite and 750°C for both studied *cis*-vacant montmorillonite and *trans*-vacant illite. During calcination, kaolinite was transformed into X-ray amorphous metakaolinite. Metamontmorillonite and metaillite were not X-ray amorphous after calcination. Dissolution was incomplete for all metaclay minerals. Metakaolinite showed the highest solubility after 24 h compared to both calcined materials containing 2:1 layer silicates. The solubility of the metaclay minerals decreased in the order metakaolinite > metamontmorillonite > metaillite. While metakaolinite (700°C) and metaillite (750°C) showed congruent dissolution, metamontmorillonite (750°C) showed incongruent dissolution. While the distribution of octahedral vacancies in 2:1 layer minerals strongly influenced the dehydroxylation temperature, optimal activation temperature was similar and solubility was influenced by chemical composition and turbostratic disorder.

Dissolution characteristics of the raw materials with respect to Si:Al were similar to the materials calcined at 900°C and higher. The uncalcined samples showed very low solubilities (<30 mol.% Si) independent of the type of clay mineral. Calcination at temperatures significantly higher than 750°C led to decreased solubility for the metamontmorillonite as well as for the metaillite, while metakaolinite still showed high dissolution after calcination at 900°C.

$Al(OH)_3$ showed almost complete solubility up to 89 mol.% Al in 10.79 mol/L NaOH after 24 h and would be suitable to adjust the Si:Al ratio for geopolymer production. To optimize the dissolution in lower NaOH concentrations, a longer reaction time up to 7 days, i.e. pre-

solution prior to mixing the precursors, should be considered for $Al(OH)_3$.

Furthermore, the lateral dimension of the layers of the clay minerals (e.g. the specific surface area and accessible edge surface) influenced the solubility. The comparison of the solubility of two different metakaolinites showed that the metakaolinite with the larger specific surface area was dissolved to a greater extent. The same trend was observed for the solubility of two different metamontmorillonites. The results of the solubility experiments and first tests on geopolymer production in water glass ($Na_{2x}Si_yO_{2y+x}$) free systems led to the assumption that all three clay minerals are suitable as precursors. Different amounts of unreacted metaclay minerals in the hardened binders are expected, which supposedly will influence the mechanical properties of the resulting geopolymers.

Supplementary Information The online version contains supplementary material available at https://doi.org/10.1007/s42860-022-00185-6.

Acknowledgments This project was funded by Deutsche Forschungsgemeinschaft under EM79/8-1. The ICP-OES measurements were performed with the help of Chantalle Kotschenreuther (Institute of Applied Geoscience, Karlsruhe Institute of Technology (KIT), Karlsruhe, Germany) and Silke Berberich (Competence Center for Material Moisture (CMM), Karlsruhe Institute of Technology (KIT), Karlsruhe, Germany). XRF measurements were performed by Nora Groschopf (Johannes Gutenberg-Universität, Mainz, Germany). The authors thank Yi-Yu Liu (CMM) for preparation of AFM samples by spin coating. AFM measurements were performed by Peter Krolla (Institute of Functional Interfaces, Karlsruhe Institute of Technology (KIT), Karlsruhe, Germany). The authors would like to express their sincere thanks to the reviewers for their very helpful comments and suggestions.

Authors' contributions Not applicable.

Funding Open Access funding enabled and organized by Projekt DEAL. This project is funded by Deutsche Forschungsgemeinschaft under EM79/8-1.

Data Availability The authors confirm that the data supporting the findings of this study are available within the article and its supplementary materials.

Declarations

Ethics approval and Consent to participate Not applicable.

Consent for publication Not applicable.

Competing interests The authors declare that they have no conflict of interest.

References

Amram, K., & Ganor, J. (2005). The combined effect of pH and temperature on smectite dissolution rate under acidic conditions. *Geochimica et Cosmochimica Acta, 69*(10), 2535–2546.

Assemi, S., Sharma, S., Tadjiki, S., Prisbrey, K., Ranville, J., & Miller, J. D. (2015). Effect of surface charge and elemental composition on the swelling and delamination of montmorillonite nanoclays using sedimentation field–flow fractionation and mass spectroscopy. *Clays and Clay Minerals, 63*(6), 457–468.

Badogiannis, E., Kakali, G., & Tsivilis, S. (2005). Metakaolin as supplementary cementitious material: Optimization of kaolin to metakaolin conversion. *Journal of Thermal Analysis and Calorimetry, 81*(2), 457–462.

Bauer, A., & Berger, G. (1998). Kaolinite and smectite dissolution rate in high molar KOH solutions at 35 and 80 C. *Applied Geochemistry, 13*(7), 905–916.

Bauer, A., & Velde, B. (1999). Smectite transformation in high molar KOH solutions. *Clay Minerals, 34*(2), 259–273.

Bauer, A., Velde, B., & Berger, G. (1998). Kaolinite transformation in high molar KOH solutions. *Applied Geochemistry, 13*(5), 619–629.

Brunauer, S., Emmett, P. H., & Teller, E. (1938). Adsorption of gases in multimolecular layers. *Journal of the American Chemical Society, 60*(2), 309–319.

Buchwald, A., Hohmann, M., Posern, K., & Brendler, E. (2009). The suitability of thermally activated illite/smectite clay as raw material for geopolymer binders. *Applied Clay Science, 46*(3), 300–304.

Carroll-Webb, S. A., & Walther, J. V. (1988). A surface complex reaction model for the pH–dependence of corundum and kaolinite dissolution rates. *Geochimica et Cosmochimica Acta, 52*(11), 2609–2623.

Charlet, L., Alt-Epping, P., Wersin, P., & Gilbert, B. (2017). Diffusive transport and reaction in clay rocks: A storage (nuclear waste, CO_2, H_2), energy (shale gas) and water quality issue. *Advances in Water Resources, 106*, 39–59.

Chermak, J. (1992). Low temperature experimental investigation of the effect of high pH NaOH solutions on the Opalinus Shale, Switzerland. *Clays and Clay Minerals, 40*, 650–650.

Cuevas, J., De La Villa, R. V., Ramírez, S., Sánchez, L., Fernández, R., & Leguey, S. (2006). The alkaline reaction of FEBEX bentonite: A contribution to the study of the performance of bentonite/concrete engineered barrier systems. *Journal of Iberian Geology, 32*(2), 151–174.

De Windt, L., Deneele, D., & Maubec, N. (2014). Kinetics of lime/bentonite pozzolanic reactions at 20 and 50 C: Batch tests and modeling. *Cement and Concrete Research, 59*, 34–42.

Delavernhe, L., Steudel, A., Darbha, G., Schäfer, T., Schuhmann, R., Wöll, C., Geckeis, H., & Emmerich, K. (2015). Influence of mineralogical and morphological properties on the cation exchange behavior of dioctahedral smectites. *Colloids and Surfaces A: Physicochemical and Engineering Aspects, 481*, 591–599.

Dietel, J., Warr, L. N., Bertmer, M., Steudel, A., Grathoff, G. H., & Emmerich, K. (2017). The importance of specific surface area in the geopolymerization of heated illitic clay. *Applied Clay Science, 139*, 99–107.

Doebelin, N., & Kleeberg, R. (2015). Profex: A graphical user interface for the Rietveld refinement program BGMN. *Journal of Applied Crystallography, 48*(5), 1573–1580.

Dohrmann, R., Kaufhold, S., & Lundqvist, B. (2013). The role of clays for safe storage of nuclear waste. In F. Bergaya & G. Lagaly (Eds.). *Developments in Clay Science, 5*, 677–710.

Drits, V., Besson, G., & Muller, F. (1995). An improved model for structural transformation of heat–treated aluminous dioctahedral 2: 1 layer silicates. *Clays and Clay Minerals, 43*(6), 718–731.

Duxson, P., Provis, J. L., Lukey, G. C., Mallicoat, S. W., Kriven, W. M., & Van Deventer, J. S. (2005). Understanding the relationship between geopolymer composition, microstructure and mechanical properties. *Colloids and Surfaces A: Physicochemical and Engineering Aspects, 269*(1–3), 47–58.

Elert, K., Pardo, E. S., & Rodriguez–Navarro, C. (2015). Mineralogical evolution of di–and trioctahedral smectites in highly alkaline environments. *Clays and Clay Minerals, 63*(6), 414–431.

Elzea, J., Odom, I., & Miles, W. (1994). Distinguishing well ordered opal-CT and opal-C from high temperature cristobalite by X-ray diffraction. *Analytica Chimica Acta, 286*(1), 107–116.

Emmerich, K., Wolters, F., Kahr, G., & Lagaly, G. (2009). Clay profiling: The classification of montmorillonites. *Clays and Clay Minerals, 57*(1), 104–114.

Fernández, R., Cuevas, J., Sánchez, L., de la Villa, R. V., & Leguey, S. (2006). Reactivity of the cement–bentonite interface with alkaline solutions using transport cells. *Applied Geochemistry, 21*(6), 977–992.

Fletcher, R. A., MacKenzie, K. J., Nicholson, C. L., & Shimada, S. (2005). The composition range of aluminosilicate geopolymers. *Journal of the European Ceramic Society, 25*(9), 1471–1477.

Garg, N., & Skibsted, J. (2015). Heated montmorillonite: Structure, reactivity, and dissolution. *Calcined clays for sustainable concrete* (pp. 117–124).

Garg, N., & Skibsted, J. (2019). Dissolution kinetics of calcined kaolinite and montmorillonite in alkaline conditions: Evidence for reactive Al (V) sites. *Journal of the American Ceramic Society, 102*(12), 7720–7734.

Glass, H. D. (1954). High–temperature phases from kaolinite and halloysite. *American Mineralogist: Journal of Earth and Planetary Materials, 39*(3–4), 193–207.

Grathoff, G. H., & Moore, D. (1996). Illite polytype quantification using WILDFIRE [C] calculated X–ray diffraction patterns. *Clays and Clay Minerals, 44*(6), 835–842.

Grim, R. E., & Kulbicki, G. (1961). Montmorillonite: High temperature reactions and classification. *American Mineralogist: Journal of Earth and Planetary Materials, 46*(11–12), 1329–1369.

Güven, N. (1990). Longevity of bentonite as buffer material in a nuclear–waste repository. *Engineering Geology, 28*(3–4), 233–247.

He, C., Makovicky, E., & Øsbæck, B. (1995a). Thermal stability and pozzolanic activity of calcined illite. *Applied Clay Science, 9*(5), 337–354.

He, C., Osbaeck, B., & Makovicky, E. (1995b). Pozzolanic reactions of six principal clay minerals: Activation, reactivity assessments and technological effects. *Cement and Concrete Research, 25*(8), 1691–1702.

Hillier, S., & Lumsdon, D. (2008). Distinguishing opaline silica from cristobalite in bentonites: A practical procedure and perspective based on NaOH dissolution. *Clay Minerals, 43*(3), 477–486.

Honty, M., De Craen, M., Wang, L., Madejová, J., Czímerová, A., Pentrák, M., Striček, I., & Van Geet, M. (2010). The effect of high pH alkaline solutions on the mineral stability of the Boom Clay – Batch experiments at 60°C. *Applied Geochemistry, 25*(6), 825–840.

Hu, N., Bernsmeier, D., Grathoff, G. H., & Warr, L. N. (2017). The influence of alkali activator type, curing temperature and gibbsite on the geopolymerization of an interstratified illite–smectite rich clay from Friedland. *Applied Clay Science, 135*, 386–393.

Huertas, F. J., Chou, L., & Wollast, R. (1999). Mechanism of kaolinite dissolution at room temperature and pressure. Part II: Kinetic study. *Geochimica et Cosmochimica Acta, 63*(19–20), 3261–3275.

Izadifar, M., Thissen, P., Steudel, A., Kleeberg, R., Kaufhold, S., Kaltenbach, J., Schuhmann, R., Dehn, F., & Emmerich, K. (2020). Comprehensive examination of dehydroxylation of kaolinite, disordered kaolinite, and dickite: Experimental studies and Density Functional Theory. *Clays and Clay Minerals, 68*(4), 319–333.

Janek, M., Komadel, P., & Lagaly, G. (1997). Effect of autotransformation on the layer charge of smectites determined by the alkylammonium method. *Clay Minerals, 32*(4), 623–632.

Karnland, O., Olsson, S., Nilsson, U., & Sellin, P. (2007). Experimentally determined swelling pressures and geochemical interactions of compacted Wyoming bentonite with highly alkaline solutions. *Physics and Chemistry of the Earth, Parts A/B/C, 32*(1–7), 275–286.

Kayabali, K. (1997). Engineering aspects of a novel landfill liner material: Bentonite–amended natural zeolite. *Engineering Geology, 46*(2), 105–114.

Khalifa, A. Z., Pontikes, Y., Elsen, J., & Cizer, Ö. (2019). Comparing the reactivity of different natural clays under thermal and alkali activation. *RILEM Technical Letters, 4*, 74–80.

Khalifa, A. Z., Cizer, Ö., Pontikes, Y., Heath, A., Patureau, P., Bernal, S. A., & Marsh, A. T. (2020). Advances in alkali–activation of clay minerals. *Cement and Concrete Research, 132*, 106050.

Köhler, S. J., Dufaud, F., & Oelkers, E. H. (2003). An experimental study of illite dissolution kinetics as a function of pH from 1.4 to 12.4 and temperature from 5 to 50°C. *Geochimica et Cosmochimica Acta, 67*(19), 3583–3594.

Kuwahara, Y. (2006). In-situ AFM study of smectite dissolution under alkaline conditions at room temperature. *American Mineralogist, 91*(7), 1142–1149.

Locati, F., Marfil, S., Baldo, E., & Maiza, P. (2010). Na_2O, K_2O, SiO_2 and Al_2O_3 release from potassic and calcic–sodic feldspars into alkaline solutions. *Cement and Concrete Research, 40*(8), 1189–1196.

Madsen, F. T. (1998). Clay mineralogical investigations related to nuclear waste disposal. *Clay Minerals, 33*(1), 109–129.

McConville, C. J., & Lee, W. E. (2005). Microstructural development on firing illite and smectite clays compared with that in kaolinite. *Journal of the American Ceramic Society, 88*(8), 2267–2276.

Metz, V., Amram, K., & Ganor, J. (2005). Stoichiometry of smectite dissolution reaction. *Geochimica et Cosmochimica Acta, 69*(7), 1755–1772.

Mosser-Ruck, R., & Cathelineau, M. (2004). Experimental transformation of Na, Ca-smectite under basic conditions at 150°C. *Applied Clay Science, 26*(1–4), 259–273.

Nagy, K. L. (2018). Chemical weathering rates of silicate minerals. In F. W. Arthur & L. B. Susan (Eds.), *Chapter 5. Dissolution and precipitation kinetics of sheet silicates* (pp. 173–234).

Nakayama, S., Sakamoto, Y., Yamaguchi, T., Akai, M., Tanaka, T., Sato, T., & Iida, Y. (2004). Dissolution of montmorillonite in compacted bentonite by highly alkaline aqueous solutions and diffusivity of hydroxide ions. *Applied Clay Science, 27*(1), 53–65.

Nikolov, A., Rostovsky, I., & Nugteren, H. (2017). Geopolymer materials based on natural zeolite. *Case Studies in Construction Materials, 6*, 198–205.

Pabalan, R. T., & Pitzer, K. S. (1987). Thermodynamics of NaOH (aq) in hydrothermal solutions. *Geochimica et Cosmochimica Acta, 51*(4), 829–837.

Pereira, J. A., Schwaab, M., Dell'Oro, E., Pinto, J. C., Monteiro, J. L., & Henriques, C. A. (2009). The kinetics of gibbsite dissolution in NaOH. *Hydrometallurgy, 96*(1–2), 6–13.

Rozalén, M. L., Huertas, F. J., Brady, P. V., Cama, J., García-Palma, S., & Linares, J. (2008). Experimental study of the effect of pH on the kinetics of montmorillonite dissolution at 25°C. *Geochimica et Cosmochimica Acta, 72*(17), 4224–4253.

Rozalen, M., Huertas, F. J., & Brady, P. V. (2009). Experimental study of the effect of pH and temperature on the kinetics of montmorillonite dissolution. *Geochimica et Cosmochimica Acta, 73*(13), 3752–3766.

Sato, T., Kuroda, M., Yokoyama, S., Fukushi, K., Tanaka, T., & Nakayama, S. (2003). Mechanism and kinetics of smectite dissolution under alkaline conditions. *Geochimica et Cosmochimica Acta, 67*(18), A415.

Sato, T., Kuroda, M., Yokoyama, S., Tsutsui, M., Pacau, C., Ringor, C., Fukushi, K., Tanaka, T., & Nakayama, S. (2005). Dissolution kinetics of smectite under alkaline conditions. *Clays in Natural and Engineered Barriers for Radioactive Waste Confinement.* Int. Meeting, March, 14–18, Tours, France.

Seiffarth, T., Hohmann, M., Posern, K., & Kaps, C. (2013). Effect of thermal pre-treatment conditions of common clays on the performance of clay-based geopolymeric binders. *Applied Clay Science, 73*, 35–41.

Shubbar, A. A., Sadique, M., Kot, P., & Atherton, W. (2019). Future of clay–based construction materials – A review. *Construction and Building Materials, 210*, 172–187.

Sonuparlak, B., Sarikaya, M., & Aksay, I. A. (1987). Spinel phase formation during the 980°C exothermic reaction in the kaolinite-to-mullite reaction series. *Journal of the American Ceramic Society, 70*(11), 837–842.

Steudel, A., Batenburg, L. F., Fischer, H. R., Weidler, P. G., & Emmerich, K. (2009a). Alteration of non–swelling clay minerals and magadiite by acid activation. *Applied Clay Science, 44*(1), 95–104.

Steudel, A., Batenburg, L. F., Fischer, H. R., Weidler, P. G., & Emmerich, K. (2009b). Alteration of swelling clay minerals by acid activation. *Applied Clay Science, 44*(1), 105–115.

Stevens, R. (1946). A system for calculating analyses of micas and related minerals to end members. *U.S. Geological Survey Bulletin, 950*, 101–119.

Tregger, N. A., Pakula, M. E., & Shah, S. P. (2010). Influence of clays on the rheology of cement pastes. *Cement and Concrete Research, 40*(3), 384–391.

Valenzuela Díaz, F. R., & Santos, P. d. S. (2001). Studies on the acid activation of Brazilian smectitic clays. *Química Nova, 24*, 345–353.

Werling, N., Dehn, F., Krause, F., Steudel, A., Schuhmann, R., & Emmerich, K. (2020). Solubility of precursors and carbonation of waterglass-free geopolymers. *Clays and Clay Minerals, 68*(5), 524–531.

Wolters, F., & Emmerich, K. (2007). Thermal reactions of smectites—Relation of dehydroxylation temperature to octahedral structure. *Thermochimica Acta, 462*(1–2), 80–88.

Wolters, F., Lagaly, G., Kahr, G., Nueesch, R., & Emmerich, K. (2009). A comprehensive characterization of dioctahedral smectites. *Clays and Clay Minerals, 57*(1), 115–133.

Xu, H., & Van Deventer, J. (2000). The geopolymerisation of alumino–silicate minerals. *International Journal of Mineral Processing, 59*(3), 247–266.

Zysset, M., & Schindler, P. W. (1996). The proton promoted dissolution kinetics of K–montmorillonite. *Geochimica et Cosmochimica Acta, 60*(6), 921–931.